Molecular-scale structural and functional characterization of sparsely tethered bilayer lipid membranes

Duncan J. McGillivray[a)]
Department of Physics, Carnegie Mellon University, Pittsburgh, Pennsylvania 15213 and National Institute of Standards and Technology (NIST), Center for Neutron Research, 100 Bureau Drive, Gaithersburg, Maryland 20899

Gintaras Valincius
Institute of Biochemistry, Mokslininku 12, LT-08662 Vilnius, Lithuania

David J. Vanderah and Wilma Febo-Ayala
Biochemical Sciences Division, NIST Chemical Science and Technology Laboratory, 100 Bureau Drive, Gaithersburg, Maryland 20899

John T. Woodward
Optical Technology Division, NIST Physics Laboratory, 100 Bureau Drive, Gaithersburg, Maryland 20899

Frank Heinrich
Department of Physics, Carnegie Mellon University, Pittsburgh, Pennsylvania 15213 and National Institute of Standards and Technology (NIST), Center for Neutron Research, 100 Bureau Drive, Gaithersburg, Maryland 20899

John J. Kasianowicz
Semiconductor Electronics Division, NIST Electronics and Electrical Engineering Laboratory, 100 Bureau Drive, Gaithersburg, Maryland 20899

Mathias Lösche[b)]
Department of Physics, Carnegie Mellon University, Pittsburgh, Pennsylvania 15213 and National Institute of Standards and Technology (NIST), Center for Neutron Research, 100 Bureau Drive, Gaithersburg, Maryland 20899

Surface-tethered biomimetic bilayer membranes (tethered bilayer lipid membranes (tBLMs)) were formed on gold surfaces from phospholipids and a synthetic 1-thiahexa(ethylene oxide) lipid, WC14. They were characterized using electrochemical impedance spectroscopy, neutron reflection (NR), and Fourier-transform infrared reflection-absorption spectroscopy (FT-IRRAS) to obtain functional and structural information. The authors found that electrically insulating membranes (conductance and capacitance as low as 1 μS cm^{-2} and 0.6 μF cm^{-2}, respectively) with high surface coverage ($>95\%$ completion of the outer leaflet) can be formed from a range of lipids in a simple two-step process that consists of the formation of a self-assembled monolayer (SAM) and bilayer completion by "rapid solvent exchange." NR provided a molecularly resolved characterization of the interface architecture and, in particular, the constitution of the space between the tBLM and the solid support. In tBLMs based on SAMs of pure WC14, the hexa(ethylene oxide) tether region had low hydration even though FT-IRRAS showed that this region is structurally disordered. However, on mixed SAMs made from the coadsorption of WC14 with a short-chain "backfiller," β-mercaptoethanol, the submembrane spaces between the tBLM and the substrates contained up to 60% exchangeable solvent by volume, as judged from NR and contrast variation of the solvent. Complete and stable "sparsely tethered" BLMs (stBLMs) can be readily prepared from SAMs chemisorbed from solutions with low WC14 proportions. Phospholipids with unsaturated or saturated, straight or branched chains all formed qualitatively similar stBLMs. © *2007 American Vacuum Society.* [DOI: 10.1116/1.2709308]

I. INTRODUCTION

The molecular organization of biological membranes and their interactions with the extracellular and intracellular spaces are critical determinants of cell function. The assessment of these features is essential to molecular medicine, is critical for an understanding of toxin mechanisms and the design of biosensor devices, and is a focus of current research in molecular biophysics.[1] However, the intrinsic complexity of the cell membrane system, a very specific molecular architecture of lipids, sterols, proteins, glycolipids, etc., often precludes direct access to these features, thus driving the development of simpler model systems that are more amenable to a detailed characterization. One generic

---

[a)]Present address: Research School of Chemistry, The Australian National University, Canberra, ACT 0200, Australia.
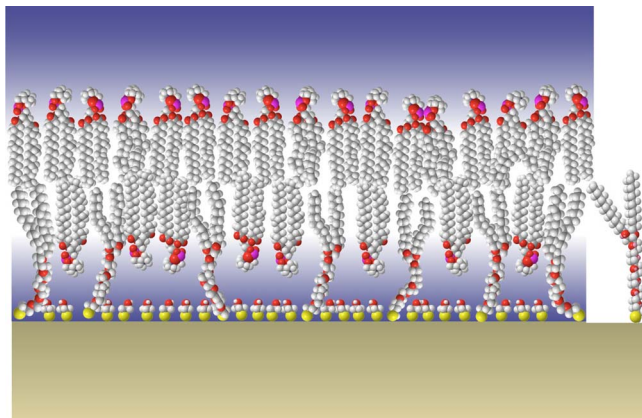[b)]Author to whom correspondence should be addressed; electronic mail: quench@cmu.edu

FIG. 1. Illustration of an stBLM such as those investigated here. A molecular model of 20-tetradecyloxy-3,6,9,12,15,18,22-heptaoxahexatricontane-1-thiol (WC14) with its HEO spacer in the extended *all-trans* conformation is given on the right.

approach,[1–4] adopted in various implementations,[5–17] involves solid supports for the stabilization of biomimetic membranes. Such platforms are more and more frequently used for practical applications.[5,18,19] Planar surfaces, particularly if they are electrically conducting, are advantageous as they allow investigations with surface-sensitive characterization techniques such as ellipsometry, neutron or x-ray reflection, surface plasmon resonance (SPR), scanning probe microscopy (e.g., atomic force microscopy), or electrical impedance spectroscopy (EIS). They also impart robustness and resilience to the membrane structures that is necessary for biotechnological applications. While there are numerous implementations of solid-supported membranes,[5,6,9] most of these approaches have not resolved the molecular-scale details of the membrane architecture. By contrast, the aim of the work reported here is the design and optimization of a tethered bilayer lipid membrane (tBLM) system that includes a comprehensive molecular-level structural and functional characterization. This article focuses on a membrane system, illustrated in Fig. 1, that is chemically tethered to the support through a synthetic lipid. The advantages of such an approach are discussed below.

Synthetic lipids involved in a generic approach to surface chemistry that is also utilized in this work often adhere to a design that incorporates the following building blocks: [chemical linker to surface]–[hydrophilic polymer tether]–[lipid backbone]–[lipid tail(s)]. A significant advantage of covalently bonding to the surface is that such an approach inhibits detachment which may be a problem for physisorbed membranes formed from vesicle fusion, e.g., under the influence of electric fields.[20] A convenient and commonly used chemisorption method is the sulfur-gold bond, e.g., using a thiol or disulfide/lipoic acid end group, which forms rapidly at room temperature and leads to reproducible self-assembled monolayers (SAMs) with long-term stability. Moreover, the presence of the metallic Au surface is particularly desirable for some surface characterization techniques
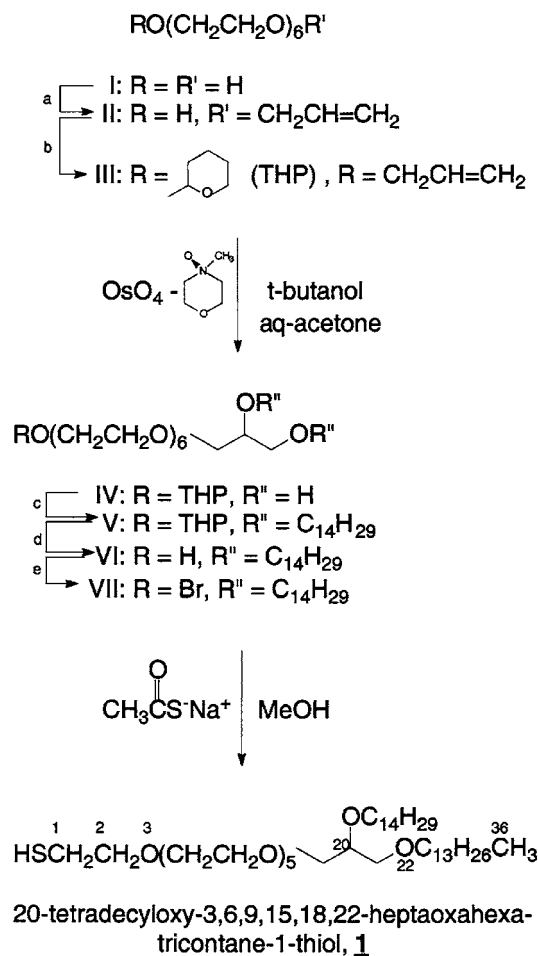
(e.g., SPR) and also provides a surface electrode for electrochemical studies or manipulations of the surface through electrostatic fields.

The hydrophilic oligomer section of the synthetic lipid, often an oligo(ethylene oxide) (OEO) segment, is designed to provide a physical separation of the membrane from the solid surface while allowing the region between the membrane and the solid surface ("submembrane space") to incorporate an aqueous reservoir. This aqueous reservoir maintains the inner surface of the membrane in a biologically relevant hydration state, similar to that brought about by the cytosol. It is critical that the tBLM be able to accommodate transmembrane protein hydrophilic segments present on either or both sides of the biomembrane. Again, the presence of such a reservoir is a major advantage of the tBLM over a physisorbed bilayer, as the water reservoir underneath those is usually <10 Å thick.[21]

The submembrane reservoir in tBLMs has not previously been structurally characterized on the molecular scale, although its presence has been inferred from electrochemical characterization, particularly by Cornell and co-workers who used a complex SAM.[22–24] The system presented here is practically much simpler and allows better control of the hydration and thickness of the submembrane space, which has been directly probed using neutron reflectometry (NR).

The hydrophobic tail region of the synthetic lipid allows for further control of the self-assembly and electrical characteristics of the membranes. Different approaches have used single chains,[25] double chains modeled after physiological lipids, or branched chains (phytanyl)[26] derived from particularly stable thermophilic bacterial membranes. We chose a pair of C_{14} *n*-alkyl chains for synthetic simplicity and greater flexibility of the chains than that offered by phytanyl chains.

In terms of structural investigations of lipid membrane models by scattering techniques, the tBLM approach described here provided the basis for a breakthrough because of its resilience and long-term stability. These properties permitted us to use one physical substrate (Si wafer with oxide layer, Cr bonding layer, and Au film of ~100 Å thickness) to form a tethered SAM and complete bilayer (see Sec. II) and to characterize the sample sequentially at various stages of this preparation procedure under various solvent contrasts. Specifically, the samples were sufficiently robust to permit exchange of the adjacent buffer phase *in situ* on the neutron spectrometer, such that the neutron beam impinged on the same physical area on the substrate in runs with different neutron contrasts. Even if the complex substrate structure was somewhat inhomogeneous in plane (we verified with x-ray reflectometry and ellipsometry that this is not the case, see below), this would justify the refinement of various related neutron spectra at different contrasts with *one* set of parameters that describes the properties of the substrate, which are invariant to solvent exchange. Not only does this technology greatly facilitate the identification of unique neutron scattering length density (nSLD) profiles; as we show in a separate paper,[27] this technique also permits structural investigations of proteins associated with sparsely tethered bi-

RO(CH$_2$CH$_2$O)$_6$R'

a ⟶ I: R = R' = H
      II: R = H, R' = CH$_2$CH=CH$_2$

b ⟶ III: R = (THP) , R = CH$_2$CH=CH$_2$

OsO$_4$ - [N-CH$_3$]   t-butanol
                        aq-acetone

↓

RO(CH$_2$CH$_2$O)$_6$—CH(OR")—CH$_2$OR"

c ⟶ IV: R = THP, R" = H
d ⟶ V: R = THP, R" = C$_{14}$H$_{29}$
e ⟶ VI: R = H, R" = C$_{14}$H$_{29}$
      VII: R = Br, R" = C$_{14}$H$_{29}$

CH$_3$C(=O)S$^-$Na$^+$ MeOH

↓

HSCH$_2$CH$_2$O(CH$_2$CH$_2$O)$_5$ ... OC$_{14}$H$_{29}$ / OC$_{13}$H$_{26}$CH$_3$

20-tetradecyloxy-3,6,9,15,18,22-heptaoxahexa-tricontane-1-thiol, 1

SCHEME 1. Overview of the synthesis of 20-tetradecyloxy-3,6,9,12,15,18,22-heptaoxahexatricontane-1-thiol, WC14. (a) NaH/THF then CH$_2$=CHCH$_2$Br; (b) 3,4-dihydro-2H-pyran, H$^+$/CHCl$_3$; (c) KOH/C$_6$H$_6$, then tetradecylmesylate; (d) H$^+$/THF-H$_2$O; and (e) trifluoroacetic anhydride/THF, then LiBr/THF-HMPA. A more complete description and product characterization is given in the Supplementary Information (Ref. 29).

layer lipid membranes (stBLMs) at unprecedented resolution by enabling characterization of the membrane before and after exposure to protein.

II. MATERIALS AND METHODS (SEE REF. 28)

A. Materials

A 1-thiahexa(ethylene oxide) lipid, 20-tetradecyloxy-3,6,9,12,15,18,22-heptaoxahexatricontane-1-thiol (WC14), was synthesized, purified, and characterized in house (Sch. 1; for full details see Ref. 29). The phospholipids, DPhyPC: 1,2-diphytanoyl-*sn*-glycero-3-phosphocholine; DOPC: 1,2-dioleoyl-*sn*-glycero-3-phosphocholine; POPC: 1-palmitoyl-2-oleoyl-*sn*-glycero-3-phosphocholine; and DMPC: 1,2-dimyristoyl-*sn*-glycero-3-phosphocholine were used as supplied from Avanti Polar Lipids (Birmingham, AL). β-mercaptoethanol (βME) from Sigma-Aldrich (St. Louis, MO) was distilled before use. Ultrapure H$_2$O was obtained from a Millipore UHQ reagent grade water purification system. D$_2$O (99.9% isotope purity) was used as received from

Cambridge Isotopes Laboratory (Andover, MA). SAMs were formed on thin gold layers ($\sim$100 Å for NR measurements, $\sim$2,000 Å for EIS, ellipsometry and contact angle measurements), deposited by high-energy magnetron sputtering on [100]-cut Si wafers (75 mm diameter for NR, 20×40 mm^2 otherwise), on $\sim$20 Å Cr adhesion layers. The magnetron (Auto A306; BOC Edwards, UK) and sputtering method were described in detail elsewhere.[30] Gold layers typically had an RMS surface roughness of $\sim$5 Å, as measured by x-ray reflectometry (Bruker AXS, Germany), and a uniformity of their thickness across the surface of $\pm$3% or better, as determined using ellipsometry. SAMs were formed on freshly deposited gold layers immediately after breaking the magnetron vacuum.

B. Self-assembled monolayer (SAM) formation

SAMs were produced by incubating the freshly prepared gold surface with an ethanolic solution of mixed WC14:βME in molar ratios between 1:0 and 1:9, and total concentration of 0.2 mM. The wafers were incubated for 12–36 h. Contact angle and EIS measurements on selected samples showed that the SAMs were largely complete after a few minutes of incubation with only minor changes occurring over the longer incubation times. After removal of the samples from the incubation solutions they were rinsed with absolute ethanol and dried in a nitrogen stream. Once coated with a SAM, the substrates could be stored for up to one week and used after rinsing with ethanol with no significant surface degradation, as judged from contact angle measurements and functional performance. SAM-coated substrates were always dried before bilayer completion, as ellipsometry and EIS showed that contact with water perturbs the SAM and rendered bilayer formation less efficient.

C. Tethered bilayer membrane (tBLM) completion

The rapid solvent exchange technique reported by Cornell *et al.*[5] was used to complete the synthetic membrane. This method was preferred over conventional vesicle fusion because bilayer formation completed more reproducibly, as determined by EIS. Rapid solvent exchange also allows the formation of bilayers on SAMs of relatively low hydrophobicity, as is the case when a significant proportion of the hydrophilic backfiller βME is used. Finally, with rapid solvent exchange, the bilayer phase state of the lipid used for completion was found to be largely irrelevant, because the lipid is applied to the surface in organic solution (as opposed to vesicle fusion whose efficiency depends largely on the lipid phase state).

Briefly, a 10 mM solution of lipid in absolute ethanol was allowed to incubate the SAM-covered substrate for 5 min at room temperature. It was then rapidly (within 5–7 s) displaced by a large excess of aqueous buffer solution, taking care to avoid the formation of air bubbles at the surface that could disturb the SAM. In preparations on the small substrates for EIS measurements, a 60 μl droplet of the lipid solution was vigorously flushed with 15 ml of buffer, and for NR substrates $\sim$1 ml of lipid solution was flushed with

40 ml of the buffer. The buffer used was either 10 mM Tris-HCl (tris(hydroxymethyl) aminomethane-HCl) or 10 mM phosphate buffers, *p*H 7.4–7.8, containing K^+ or Na^+ salts (0.1–0.2 M). All exchanges were performed at room temperature [(21 ± 1) °C], except for NR measurements involving DMPC where the temperature was kept above 25 °C.
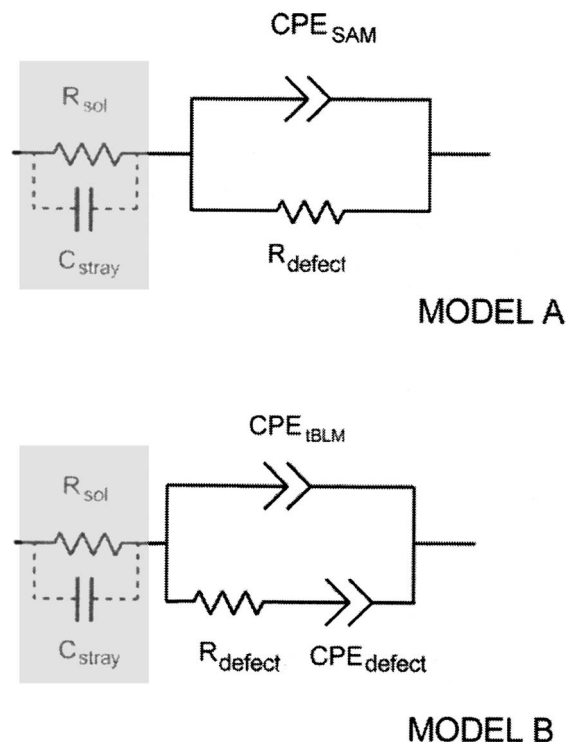
D. Electrochemical impedance spectroscopy (EIS)

EIS measurements were performed using a Solartron (Farnborough, UK) system (model 1286 potentiostat and model 1250 frequency response analyzer). Data were fitted using ZVIEW (Scribner Associates, Southern Pines, NC) to models discussed below. Spectra were obtained at frequencies between 1.0 and 65 000 Hz with ten logarithmically distributed measurements per decade. They are presented in Cole-Cole plots (Im C vs Re C, where $C = C(\omega)$ is the frequency-dependent capacitance of the electrode [31] and ω is the angular frequency, $\omega = 2\pi f$, with f the frequency in hertz). Gold-coated silicon wafers (20×40 mm^2) served as the working electrode in a setup that allowed simultaneous EIS measurements in six distinct electrochemical cells (volume $V \sim 250–300$ μl) on each wafer, with their surface areas ($A_{el} \sim 0.33$ cm^2) on the gold film confined by Viton O-rings. Copper contrast was used to measure the geometric electrode surface area.[25] EIS data were normalized to A_{el}, while the roughness factor β, estimated from the gold surface oxidation/oxide stripping charge,[32] was between 1.2 and 1.4 for different samples. A saturated silver-silver chloride [Ag|AgCl|NaCl$_{(aq,sat)}$] microelectrode (Microelectrodes, Bedford, NH, model M-401F) was used as reference. The auxiliary electrode was a 0.25 mm diameter platinum wire (99.99% purity, Aldrich) coiled around the barrel of the reference electrode. The distance between the tip of the reference and working gold electrode surface was set to 2–3 mm. All measurements were carried out at 0 V bias versus the reference electrode at (21 ± 1) °C in aerated solutions.

EI spectra were modeled using the equivalent circuit models shown in Sch. 2 for the tethered SAM (model A) and the tethered bilayer systems (model B). The relevance and significance of these models are discussed in Sec. III. Confidence limits of the best-fit model parameters were quantified by evaluating the variance-covariance matrices of the Levenberg-Marquardt algorithm employed in the nonlinear χ^2 minimization.

E. Spectroscopic ellipsometry

Multiple-wavelength ellipsometric optical thickness measurements on the SAMs were performed on a spectroscopic ellipsometer (J.A. Woollam, Lincoln, NE, model M-44), set to a nominal incidence angle of 70° from the surface normal, with the exact angle fitted (WVASE, J.A. Woollam). Ethanol-rinsed and dried SAMs were typically measured at four different locations on the substrate for each sample. To reduce noise, 3000 revolutions of the analyzer were accumulated. For reproducibility, thicknesses were determined using opti-

SCHEME 2. Equivalent circuits used in the modeling of electrochemical impedance spectra. Model A: SAM; model B: stBLM.

cal parameters derived from a deuterated *n*-octadecanethiol reference SAM on Au, as described earlier.[30] Data were modeled as a single slab with a homogeneous, isotropic optical constant on an infinite gold substrate.

F. Neutron reflectometry (NR)

NR is a surface-sensitive technique that provides molecular-scale information about the structure of interfacial layers perpendicular to the interface.[33] The measurements described in this work were performed on the Advanced Neutron Diffractometer/Reflectometer[34] (AND/R) at the NIST Center for Neutron Research. This instrument is a vertical-sample, angle-dispersive reflectometer capable of measuring reflectivities as low as 10^{-7} for a sample at the solid-liquid interface (primarily limited by sample-dependent background). Background was measured at positions of the detector offset by $0.25 \times \theta$ on both sides of the specular angle θ, and averaged.

Data analysis was performed in terms of slab models ("box" models) using GA_REFL,[35] which enables the constrained fitting of multiple data sets and takes advantage of a genetic algorithm to perform a rapid search across parameter space with robustness against trapping in local minima. Roughness of the interfaces between adjacent slabs was implemented in the model by smoothing the steps between the different nSLD values with error functions, and then subdividing the smoothed film structure into a histogram of thin slabs. The reflectivity of this model was computed using an optical matrix based on Parratt's recursion algorithm.[36]

The following models were used to describe the molecular surface architectures (see Fig. 1, as well as insets in subsequent figures, below, that present selected NR data sets). In these models, a semi-infinite Si volume (nSLD, $\rho_n = 2.1 \times 10^{-6}$ Å^{-2}) was covered by a thin layer (thickness, $d \sim 15$ Å) of SiO$_x$ ($\rho_n = 3.4 \times 10^{-6}$ Å^{-2}), followed by a thin bonding layer of sputtered Cr ($d \sim 15$ Å) and the sputtered Au film ($d \sim 100$ Å, $\rho_n = 4.5 \times 10^{-6}$ Å^{-2}). Presumably due to the energy deposition during sputtering, the bonding layer appeared to be composed of a Cr/Au alloy with $\rho_n = 4 \times 10^{-6}$ Å^{-2} in the fitted models. In the initial phase of this work, we determined the optical thickness parameters of the substrates using the in-house x-ray reflectometer in order to later on reduce the complexity of the models describing the organic surface architectures. Starting nSLD values for SiO$_x$, Cr, and Au layers were taken from tabulated data[37] and refined. The thus determined parameters of the substrates were then kept constant in the modeling of neutron data. We later found that these parameters may be equally well determined with a comparable precision from neutron scattering alone if the samples were measured at various sequential steps of the preparation, starting with a freshly prepared SAM, and corefined in one consistent model (see below). Because of the long-term stability of the supported bilayers, such measurements were carried out on one specific interfacial area of one physical sample, such that there is no doubt that the substrate structure is identical in these sequential measurements.

To describe the surface structure after SAM formation, two additional layers were added to the model. The first of these layers, closest to the gold surface, was ascribed to the hexa(ethylene oxide) (HEO) spacer and an unknown amount of water, to be determined from the simultaneous fit to data from various solvent contrasts. The second layer described an alkyl slab ($d \sim 20$ Å). The model that described a SAM was terminated with the second half-space whose nSLD was set to either reflect that of air ($\rho_n = 0$) or D$_2$O ($\rho_n \sim 6.4 \times 10^{-6}$ Å^{-2}). Finally, to model a completed tBLM, an additional alkyl slab was added to describe the full bilayer structure. The dual alkyl slab thickness, $d_{bilayer}$, was divided into two individual layers with identical thicknesses, $d_{bilayer}/2$, but different nSLD values, ρ_{alkyl}^{prox} and ρ_{alkyl}^{dist}. This distinction is significant because it was observed that particularly the distal alkyl layer changed slightly in its nSLD upon exchange of solvent. This is obviously related to incomplete formation of the bilayer, i.e., water pockets may persist in the plane of the bilayer. Similarly, changes in the nSLD of the HEO spacer layer upon isotopic variation of the buffer in contact with the tBLM indicated exchange of solvent in this layer and were used to quantify the hydration of the spacer.

The quality of the model fits to the experimental data was measured by $\chi^2 = \Sigma((R_i - R(Q_z^i))/\sigma_i)^2/(N-P)$, where N is the number of experimental data points, P is the number of adjustable parameters, and σ_i are the experimental error of R_i.

G. Infrared spectroscopy

FTIR spectra in reflection-absorption Spectroscopy (FT-IRRAS) mode were obtained on a Bruker Equinox 55 instru-

TABLE I. Properties of WC14-based SAMs as a function of composition (WC14 : βME ratio) of the adsorption solution.

Molar proportion, x_{WC14}, of WC14 (in solution) (mol %)	Contact angle ϕ (deg)	Ellipsometric thickness d_{tot} (Å)
100	115(2)	33.7(5)
90	115(2)	33.3(5)
80	113(2)	33.1(5)
70	110(2)	27.9(5)
60	105(2)	21.2(2)
50	103(1)	18.8(5)
40	99(2)	14.6(2)
30	93(2)	16.0(5)
20	86(2)	13.0(5)
10	80(2)	7.1(2)
0	<10	4.8(5)

ment (Billerica, MA) with a homebuilt external reflection accessory consisting of a wire grid polarizer (Pike Scientific, Madison, WI), a slit, and an optical laboratory jack as described earlier.[30] Spectra were obtained using 755 sample and 755 background scans (10 min collection time) at 2 cm^{-1} resolution. Spectral analysis was performed using GRAMS 386 (Galactic Industries, Salem, NH).

III. RESULTS

A. SAM and tBLM structure: Pure WC14

Pure WC14 SAMs formed rapidly from ethanolic solutions, reaching >90% completion within the first minute of incubation, and changed only moderately with extended exposure as assessed by water contact angle measurements and ellipsometry. WC14 SAMs are stable and highly hydrophobic with an average contact angle of $(115 \pm 2)°$ (Table I). In addition, they are heat resistant, as no structural changes were detected by NR after 30 min under water at 80 °C.

NR measurements of pure WC14 SAMs in contact with air and with water (D$_2$O) showed the expected stratification of the sample into a dense alkyl chain layer which covers the hydrophilic HEO spacer layer (see Fig. 2). However, we were not able to determine the alkyl layer thickness precisely because of the lack of contrast of the alkyls against air. Even if measured in D$_2$O, where high contrast between the alkyl layer and the solvent was anticipated, the physical structure is more complicated than naively expected. The adsorption of a thin gas layer from the water phase creates a region of low nSLD with high apparent surface roughness next to the alkyl interface with the solvent.[38] Such an extra layer has been included in the model (see Figs. 2 and 4 at $z \sim 30$ Å) because we noticed that a "simple" model of the SAM with $d_{alkyl} \lesssim 20$ Å, as described above, did not realistically account for the data. It interferes, however, with a precise determination of the alkyl thickness.

The EIS spectrum of a WC14 SAM is shown in Fig. 3. It exhibited a semicircular shape, consistent with the capacitive behavior of a near-ideally insulating dielectric layer. This
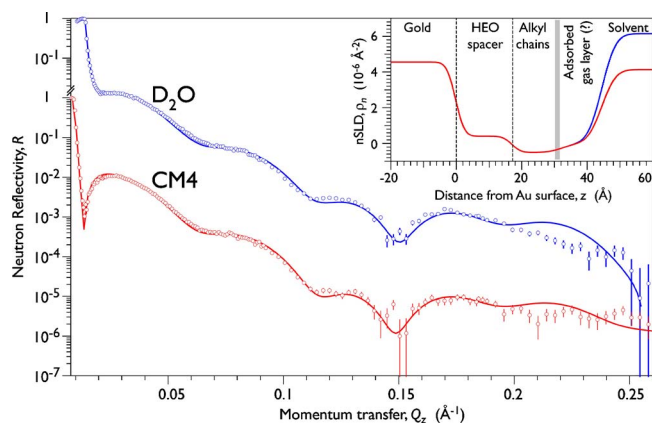
FIG. 2. NR from a 100% WC14 SAM measured in D_2O and CM4 ($D_2O:H_2O$ mixture with nSLD $\sim 4 \times 10^{-6}$ Å^{-2}). Lines derive from the fitted model (inset) of an nSLD profile composed of slabs as indicated. An adsorbed gas layer, whose approximate interface with the alkyl chains is indicated by the gray bar, reduces the nSLD between the alkane and the solvent, thus interfering with a precise determination of the alkyl layer thickness.

spectrum was well fitted to a simple equivalent circuit that is widely used for modeling dielectric properties of single-component alkanethiol SAMs (Ref. 39) and highly insulating solid-supported phospholipid bilayers [40] (model A in Sch. 2). In this scheme, constant phase element (CPE) refers to an electrical element with an impedance, $Z_{CPE} = 1/CPE(i\omega)^{\alpha}$, where CPE is the constant-phase element coefficient, mea-

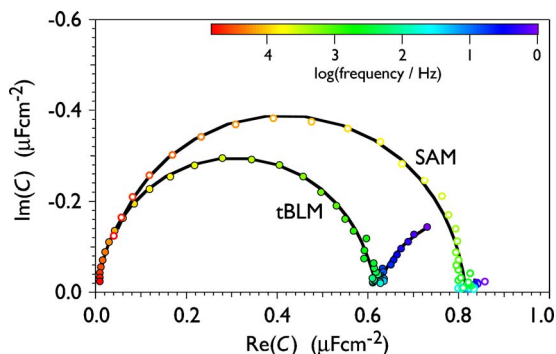FIG. 3. (a) Cole-Cole plot of the electrochemical impedance spectra, normalized to A_{el}, of a SAM ($x_{WC14}=1$) and the corresponding tBLM completed with DPhyPC. Lines are fitted models using the equivalent circuits depicted in Sch. 2. Model A was used for the SAM, while model B was used to describe the tBLM with its ohmic defects.

sured in farads per unit area $\times$ s$^{\alpha-1}$, equivalent to siemens per (unit area $\times$ Hz$^{-\alpha}$), and the exponent α varies between 0 and 1. Data modeling (Table II) showed a specific resistance R_{defect} as high as 20 MΩ cm^2, and near-ideal capacitive behavior, with $\alpha_{SAM}=1.00$, so that the total SAM capacitance could be evaluated as $C_{SAM} \approx CPE_{SAM}$. These experimental CPE_{SAM} values agree well with theoretical estimates of C_{SAM}, based on a serial two-capacitor model, representing the SAM structure in terms of the HEO and alkyl layers, and the Helmholtz capacitance of the gold/SAM interface as

$$C_{SAM} = (C_{alkyl}^{-1} + C_{HEO}^{-1} + C_H^{-1})^{-1}$$
$$= \varepsilon_0(d_{alkyl}/\varepsilon_{alkyl} + d_{HEO}/\varepsilon_{HEO} + \varepsilon_0 C_H^{-1})^{-1}, \qquad (3.1)$$

where ε_0 is the vacuum permittivity (8.85×10^{-14} F cm^{-1}) and d and ε are the thicknesses and relative permittivities of the alkyl or HEO regions, respectively. Using results for d from NR (see below) and assuming $\varepsilon_{HEO} \sim 5$ and $\varepsilon_{alkyl} \sim 2.3$,[25] and a Helmholtz capacitance, $C_H \approx 10$ μF cm^{-2},[41] yielded $C_{SAM}=0.72$ μF cm^{-2}.[41] Compared to this estimate, the measured value was $\sim 20\%$ higher, which was well accounted for by the experimentally determined roughness factor, $\beta=1.2$, of the electrode surface. The low value, $\varepsilon_{HEO} \approx 5$, used in this estimate is consistent with an almost water-free submembrane layer.

FT-IRRAS showed that pure WC14 SAMs were significantly disordered in the tether region but well ordered in the methylene region (refer to the lower half of the schematic layer structure in Fig. 1). Order in the C_{14} chains was indicated by asymmetric and symmetric methylene stretch vibration bands centered at $\nu_{as} \sim 2917$ cm^{-1} and $\nu_s \sim 2853$ cm^{-1}. These results compared favorably to the corresponding values of 2917 and 2850 cm^{-1} for polymethylene chains in the *all-trans* conformation.[42] The difference of 3 cm^{-1} in ν_s was possibly due to band overlap with methylenes in the EO segment. This band appeared as a shoulder on the more intense 2873 and 2862 cm^{-1} bands, which made a determination of its position less precise.

In contrast to the hydrophobic alkyl chains, significant disorder in the HEO segments was indicated by the broad C–O adsorption band at $\nu \sim 1131$ cm^{-1}. Similar band positions have been reported for disordered OEO segments on Au and Ag,[43] as well as for poly(ethylene glycol) in the melt at elevated temperatures.[44] In addition, this IR region lacked

TABLE II. Best-fit parameters (model A) to electrochemical impedance spectra of SAMs of various compositions. Uncertainties, in parentheses, as obtained from the covariance matrices (uncertainties in α_{SAM} were <1%). Standard errors from averaging different samples were less than 15% (CPE_{SAM}), 1% (α_{SAM}), and 30% (R_{defect}).

Parameter	Molar proportion, x_{WC14}, of WC14 (in solution)					
	100%	80%	70%	60%	50%	30%
CPE_{SAM} (μF cm^{-2} s$^{(\alpha-1)}$)	0.84(1)	0.86(1)	1.11(1)	6.17(2)	8.57(2)	9.23(4)
α_{SAM}	1.00	1.00	1.00	0.99	0.99	0.98
R_{defect}, (MΩ cm^2)	20(1)	2.65(32)	3.58(51)	2.19(69)	0.47(3)	0.51(9)
Fit quality χ^2 ($\times 10^5$)	39.9	6.79	11.8	4.53	2.25	10.3

TABLE III. Properties of tBLMs of various compositions based on mixed WC14:βME SAMs, as obtained from slab model interpretations of NR data. Best-fit parameter values given for tBLMs of pure WC14 and stBLMs with 50:50 molar proportion of WC14:βME in the adsorption solution are in most cases based on one or two measurements. In distinction, stBLMs with 30:70 WC14:βME were for some filler lipids repeatedly measured with independent samples, and the indicated precision is the standard variation of these measurements.

Filler lipid	Molar proportion (solution), x_{WC14}, of WC14 for SAM formation (mol %)	Thickness of submembrane space d_{sub} (Å)[a]	Volume fraction of exch. solvent in submembrane space x_{sub}^{water} (vol %[a])	Total alkyl thickness in tBLM, $d_{bilayer}$, (Å[a])	Outer leaflet completeness η_{distal} (vol %[a])
DPhyPC	100	16.7	4	30	100
DPhyPC	50	15.1	54	36	97
POPC		15.3	56	40	99
DOPC		15.6	60	33	94
DMPC		15.0	47	30	97
DPhyPC[b]	30	13.1(18)	64(6)	31.8(19)	98(2)
POPC[b]		13.6(38)	69(9)	34.8(25)	95(8)
DOPC		14.6	59	31.9	97
DMPC[c]		16.7	74	32.6	100
DPPC[d]		17.0(9)	75(2)	32.2(52)	100(1)

[a]Typical accuracy of these measurements, dominated by the confidence limits of the model, is estimated to be $\Delta d_{sub} \sim 1$ Å, $\Delta x_{sub}^{water} \sim 2\%$, $\Delta d_{bilayer} \sim 2$ Å, and $\Delta \eta_{distal} \sim 2\%$
[b]$n=$four independent measurements.
[c]$n=$two measurements, one of which used chain-perdeuterated DMPC-d$_{54}$.
[d]$n=$three measurements, two of which used chain-perdeuterated DPPC-d$_{62}$.

the characteristic C–O modes found for EO segments in the highly ordered 7/2 helical conformation[45] or OEO segments in the *all-trans* conformation.[43]

Bilayers formed on pure WC14 SAMs by solvent exchange using DPhyPC were estimated from NR measurements to be >95% complete (Table III). The tBLM's alkyl chains were tightly packed, with a nSLD of the hydrocarbon tails close to the minimum reported for highly compressed Langmuir monolayers.[46] Despite significant disorder of the HEO tether indicated by FT-IRRAS, NR showed no exchangeable solvent between the alkyl layer and the gold electrode, as judged from measuring the same sample in two different water contrasts.

Changes in the EI spectra upon tBLM completion were consistent with a thickness increase of the dielectric interface layer. In particular, the semicircular diameter in the Cole-Cole plot, proportional to the layer capacitance, shrunk by a factor of 1.3–1.4 (Fig. 3). Concomitantly, a new feature appeared in the form of a low-frequency "tail" that was almost straight and of considerable variability in length for different samples. In most cases, the complex capacitance at 1 Hz exceeded the semicircular diameter by a factor of 1.1–2.5. These low-frequency tails cannot be adequately described by the simple equivalent circuit used for the SAM, nor an alternative circuit used by Cornell and co-workers[5,22,24] to model tBLMs containing transmembrane ion channels. However, the equivalent circuit model B (see Sch. 2), which accounts for membrane defects, described all features well.[47] Despite these membrane defects, EI spectra exhibited near-ideal capacitive behavior with modeled CPE$_{tBLM}$ exponent values, $\alpha_{tBLM} > 0.99$, and capacitance values of C_{tBLM}

$=0.66\pm0.01$ μF cm^{-2}. These results agreed well with a capacitance estimate for a tethered SAM overlaid with an additional lipid monolayer that used the NR thickness data—a 30 Å thick alkane bilayer with $\varepsilon_{alkyl}=2.1$ and a 16.7 Å thick OEO layer with $\varepsilon_{OEO}=5$—and yielded a capacitance of 0.50 μF cm^{-2}. A Helmholtz capacitance of 10 μF cm^{-2} reduced this value to 0.48 μF cm^{-2}, which matched the measured value perfectly if the independently determined β $=1.4$ was taken into account.

B. SAM and stBLM structure: Backfilled WC14 layer

To increase the hydration of submembrane space, the surface concentration of WC14 in the SAM was decreased using the smaller, hydroxy-terminated βME as coadsorbent. SAMs were formed from a mixed ethanolic solution of WC14 and βME in varying molar ratios. Because concentrations of the coadsorbents were not directly measured and may not be the same as in the incubation solution, the βME:WC14 proportions referred to below will denote solution ratios.

As the molar proportion of WC14, x_{WC14}, in the solution decreased, the hydrophobicity of the SAMs decreased from a contact angle of $(115\pm2°)$ for a 100% WC14 layer to <100° for layers from solutions with $x_{WC14} < 70\%$ WC14. However, for a 10% WC14 layer the contact angle was still $(80\pm2°)$ (Table I). This implied that WC14 influences the surface properties of the mixed SAMs strongly even if deposited from low solution ratios with βME (a βME-only monolayer is completely wetting). Ellipsometry showed that the effect of incubation time on the surface structure is minimal—the
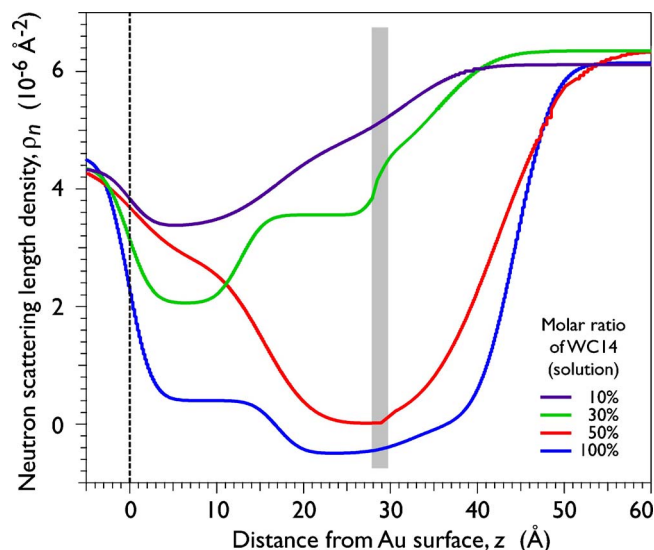
FIG. 4. nSLD profiles derived from modeling of the NR, measured in D_2O, of SAMs with varying proportions of WC14, x_{WC14}, in the adsorption solution. Adsorbed gas reduces the nSLD near the alkane/solvent interfaces, approximately indicated by the shaded bar at $z \sim 28.5$ Å. A precise determination of the alkyl/gas interface is not possible based on the NR data. The thickness of the gas layer is roughly proportional to the proportion of WC14 in the tethered layer (and hence the hydrophobicity of the SAM surface).
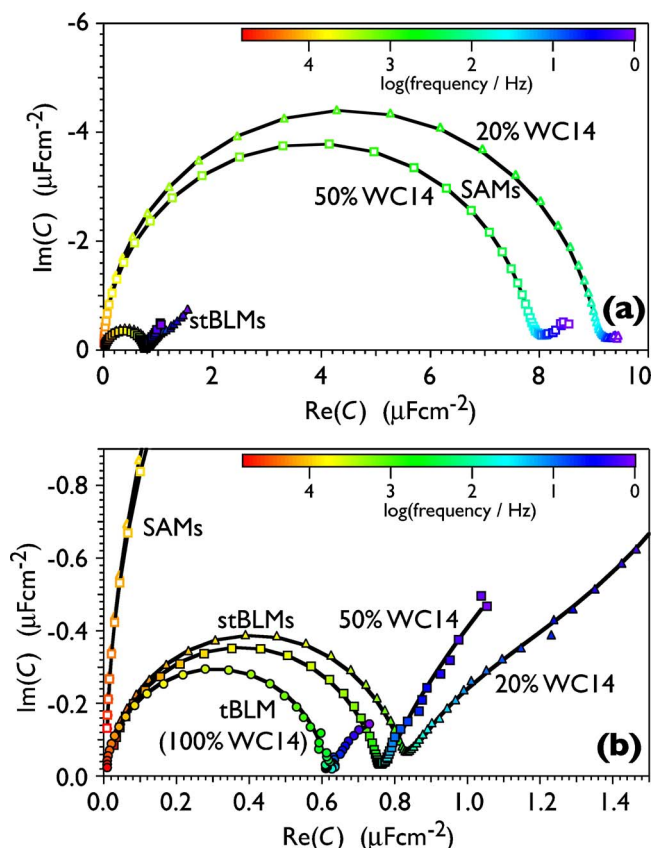

FIG. 5. Cole-Cole plots of electrochemical impedance spectra of SAMs prepared from solutions with 50% and 20% WC14, and corresponding stBLMs completed with DPhyPC. A DPhyPC tBLM prepared on a 100% WC14 SAM is shown for comparison. Panel (a) is intended to show details of the SAM spectra and visualize them in context with the vastly different tBLM spectra. Panel (b) shows an expanded view of the tBLM data. Lines are best-fit models using the equivalent circuits in Sch. 2.

increase in the ellipsometric thickness of a 50% WC14 SAM was <6% on increasing the incubation time from 24 to 190 h (data not shown).

NR on mixed SAMs in contact with water showed that the generic monolayer structure is preserved between 100% and 50% WC14, although a general increase in the nSLD of the surface film at lower WC14 concentration indicated an increased density of solvent-filled defects. At 30% WC14, however, the alkyl layer collapsed onto the surface, leading to a fundamentally distinct nSLD profile (Fig. 4). The ellipsometric thickness of the SAMs in air as a function of x_{WC14} showed an initial plateau between 100% and 80% from where it decayed and followed a linear decrease in proportion to the ratio of the components (Table I).

EI spectra of mixed SAMs changed only slightly for $100\% > x_{WC14} > 70\%$, with a slight increase in the semicircular diameter as x_{WC14} decreased. However, at $x_{WC14} \sim 70\%$ a sharp increase of the diameter of the Cole-Cole semicircle was observed (Fig. 5). The experimental capacitance values recorded at a single frequency, $C_{f=205\ Hz}$, indicated an eightfold increase, from ~ 1 to $\sim 8\ \mu F\ cm^{-2}$, of the electrode capacitance as x_{WC14} fell below 70% (Fig. 6). This was also observed in the fitted CPE_{SAM} values summarized in Table II. However, even at low x_{WC14} the model still indicated a near-ideal capacitive behavior of the interface film with $\alpha_{CPE} > 0.98$. On the other hand, the values of R_{defect} (Sch. 2) that quantify the resistance of the SAM dropped sharply once βME was introduced into the system (Table II).

Although solvent exchange with DPhyPC produced stBLMs on SAMs from WC14 $\geq 10\%$, these were affected by a significant decrease in the capacitance from that of the initial SAM (Fig. 5(a)). Bilayers formed on SAMs containing <10% WC14 were unstable, as indicated by a degradation of the electrical characteristics from those of a tBLM to
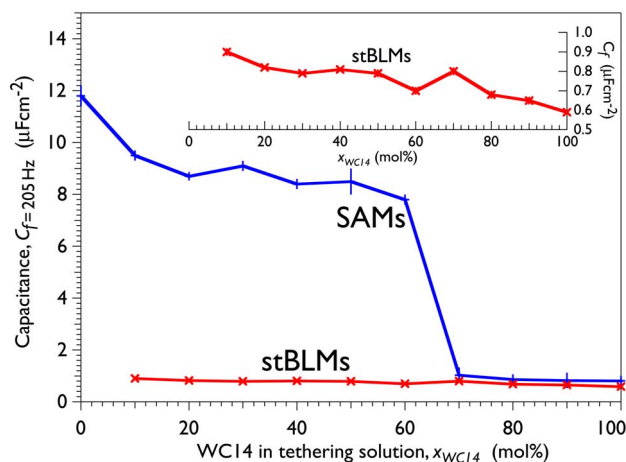

FIG. 6. SAM and stBLM capacitances, derived from the complex capacitance at a fixed frequency ($f=205$ Hz), as a function of SAM composition (proportion of WC14, x_{WC14}, in the adsorption solution). Bilayers were completed with DPhyPC. The inset shows an expanded view of the stBLM data only.
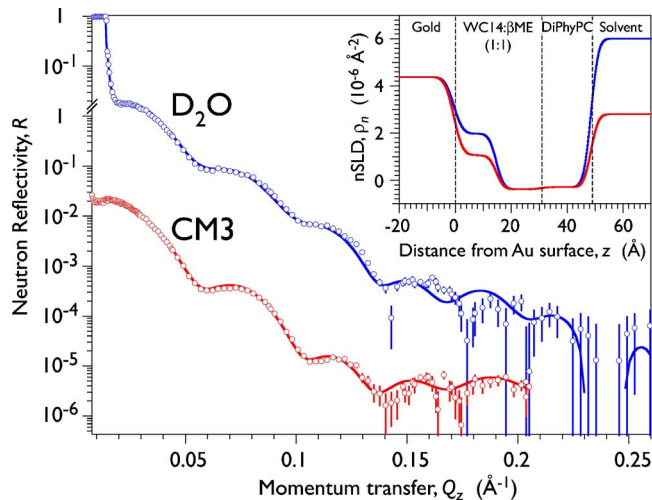
FIG. 7. NR from an stBLM ($x_{WC14}=0.5$), completed with DPhyPC, measured in D_2O and CM3 (D_2O:H_2O mixture with nSLD $\sim 3 \times 10^{-6}$ Å^{-2}). Inset: nSLD profile from a best-fit slab model to the data. Note the almost perfect completeness of layers and the change of nSLD in the submembrane space upon solvent contrast variation.

those of the underlying SAM within ~ 1 h. The electrical parameters of other membranes were stable for at least $1–2$ h and, in most cases, exhibited stability longer than 24 h.

nSLD profiles of stBLMs formed from DPhyPC on mixed SAMs were similar to those formed on 100% WC14 SAMs (Table III). Significantly, however, the NR data also showed the presence of free (exchangeable) water in the submembrane space. The water volume fraction was 47%–60%, depending on the filler lipid, for stBLMs on 50:50 WC14:βME SAMs; it was up to 70% on 30:70 WC14:βME SAMs (Table III, see also exemplary data set and nSLD profile in Fig. 7). Concomitantly with increasing hydration, the thickness of the submembrane space decreased with x_{WC14} in a systematic way, from $d_{sub} \sim 16.7$ Å ($x_{WC14}=100\%$) to ~ 13.1 Å ($x_{WC14}=30\%$). At the same time, the thickness of the alkyl/acyl bilayer increased from $d_{bilayer} \sim 30$ Å ($x_{WC14}=100\%$) with decreasing x_{WC14}. We assign this trend to the filling of voids between the WC14 alkyl tails in the chain leaflet proximal to the Au substrate with phospholipid acyl chains, which should increase the hydrophobic slab thickness.

DPhyPC-completed stBLMs exhibited roughly constant capacitance, $C_{f=205\ Hz}$, as a function of x_{WC14}, in contrast to the SAMs they were based upon. $C_{f=205\ Hz}$ values increased from 0.59 μF cm^{-2} for a tBLM on a 100% WC14 SAM to 0.90 μF cm^{-2} for the stBLM on 10% WC14 (Fig. 6). Specifically, the stBLMs did not show the sharp discontinuity in capacitance at 70% WC14 that was observed for the SAMs. Fitting EI spectra to model B indicated nearly constant values of CPE_{tBLM} (Table IV), while α_{tBLM} values decreased slightly—but remained at >0.98—as x_{WC14} decreased.

The low-frequency tails attributed to conductance pathways in the tBLM also increased in proportion (Fig. 5(b)). The resistance associated with these defects, R_{defect}, de-

TABLE IV. Best-fit parameters (model B) to electrochemical impedance spectra of DPhyPC tBLMs based on SAMs of various compositions. Uncertainties, in parentheses, as obtained from the covariance matrices.

Parameter	Molar proportion, x_{WC14}, of WC14 (in solution)			
	100%	50%	40%	30%
CPE_{tBLM} (μF cm^{-2} s$^{(\alpha-1)}$)	0.664(2)	0.827(5)	0.855(6)	0.872(7)
α_{tBLM}	0.992(2)	0.988(1)	0.986(1)	0.986(1)
CPE_{defect} (μF cm^{-2} s$^{(\alpha-1)}$)	0.56(7)	1.92(6)	1.75(4)	1.81(4)
α_{defect}	0.51(6)	0.52(3)	0.49(2)	0.48(3)
R_{defect} (kΩ cm^2)	444(100)	146(13)	124(13)	93(14)
Fit quality $\chi^2(\times 10^5)$	54	6.75	7.11	7.37

creased with x_{WC14} while the CPE exponent, α_{defect}, remained close to 0.5. In EIS theory, $\alpha=0.5$ is interpreted as an infinite RC ladder that takes into account the attenuation of the electric field along conducting pores of different geometries, as observed on porous and brush electrodes.[48,49] In tBLMs, the presence of a conducting defect causes electric field penetration into the submembrane electrolyte reservoir which gives rise to an electric field vector component that is attenuated parallel to the electrode. Its characteristic attenuation length depends on the conductivity of the submembrane space as well as the density of the defects. Low defect density results in a power law with $\alpha=0.5$; with increasing defect density, $\alpha \rightarrow 1$.[47] Similarly, CPE_{defect} reflects the electrical conductivity of the submembrane space. The greater the electric resistance of the aqueous reservoir, the lesser is the electric field penetration into this space, and consequently the smaller is CPE_{defect}. Thus both CPE_{defect} and α_{defect} suggest that stBLMs had a low defect density even for low x_{WC14}. If one assumes that ion mobility remains the same in the submembrane space as in the bulk of the electrolyte, this defect density in the tBLM may be estimated from R_{defect}. For a cylindrical pore with a length of 3 nm, a diameter of 1 nm, and an electrolyte-specific resistance of 100 Ω cm, the estimated defect densities in DPhyPC tBLMs were $\sim 7 \times 10^3$ cm^{-2} on 100% WC14 and $\sim 3.5 \times 10^4$ cm^{-2} on 30% WC14. This corresponds to volume fractions of solvent in the membrane $\ll 1\%$, which are well below the resolution of NR.

C. stBLMs completed with other lipids

To demonstrate the versatility of the mixed βME:WC14 system, stBLMs were also formed using a range of other lipids: DMPC, DOPC, and POPC. Upon bilayer formation, a decrease of the electrode capacitance was observed in all cases, consistent with an increase in dielectric layer thickness. However, as seen in Fig. 8, stBLMs completed with DMPC showed noticeably different EI spectra from those completed with DPhyPC, DOPC, or POPC. The latter lipids all formed bilayers with CPE_{tBLM} values <1 μF cm^{-2} which were stable for >24 h. (The stability varied as DPhyPC $>$ DOPC $\approx$ POPC.) The electrical characteristics of DMPC bilayers, on the other hand, reverted over a period of hours to those of the parent SAM. The Cole-Cole plots in Fig. 8 also
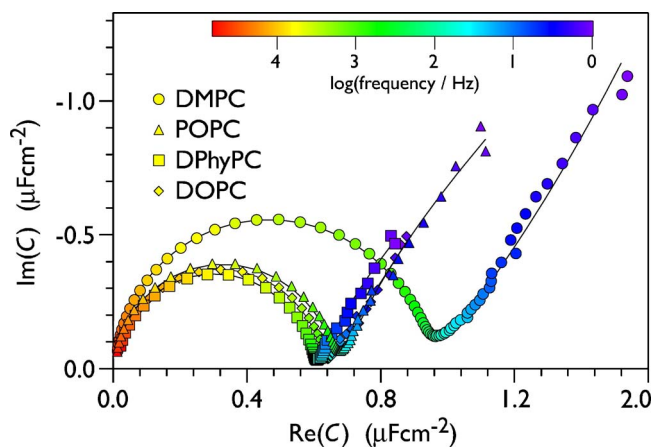
FIG. 8. Cole-Cole plots of electrochemical impedance spectra of tBLMs based on SAMs ($x_{WC14}=0.5$) that were completed with various lipids as indicated. Lines are the best-fit models using the equivalent circuit, model B.

FIG. 9. NR from an stBLM based on a SAM ($x_{WC14}=0.5$) that was completed with POPC, measured in D_2O and CM3 (D_2O:H_2O mixture with nSLD $\sim 3 \times 10^{-6}$ Å^{-2}). Inset: nSLD profile from a best-fit slab model to the data. Note the incomplete secondary bilayer at a distance of ~ 30 Å from the stBLM. This overlayer is $\sim 30\%$ complete and persisted through the exchange of the solvent phase for contrast variation.

show that the low-frequency tails, indicating Ohmic defects in the tBLM, increased in the sequence, DPhyPC $\approx$ DOPC < POPC < DMPC. Fitting parameters are summarized in Table V. CPE$_{tBLM}$ varies slightly, DPhyPC < DOPC < POPC, but is considerably higher for DMPC. This increase for DMPC cannot be explained by differences in tBLM thickness, as $d_{bilayer}^{DPhyPC}/d_{bilayer}^{DMPC} \sim 1.2$ (Table III), while CPE$_{tBLM}^{DPhyPC}$/CPE$_{tBLM}^{DMPC} \sim 1.66$ (Table V). However, R_{defect} also decreases, DPhyPC > DOPC > POPC > DMPC, dropping to 24 kΩ cm^2 for DMPC compared to 146 kΩ cm^2 for DPhyPC. Overall, the data show that DMPC tBLMs are characterized by a significantly higher dielectric constant than the remaining phospholipids.

In contrast, NR showed similar tBLM structures for all the lipids investigated and revealed structural stability over >24 h. For DMPC, the hydrophobic alkane region was observed to retain the same low overall thickness of the hydrophobic slab ($d_{bilayer} \sim 30$ Å) that is also observed for the tBLM based on 100% WC14. Any stBLM completed with another filler lipid showed larger values of $d_{bilayer}$ (Table III). This result is consistent with the assumption that the phospholipids filled in gaps between WC14 alkyl groups in the
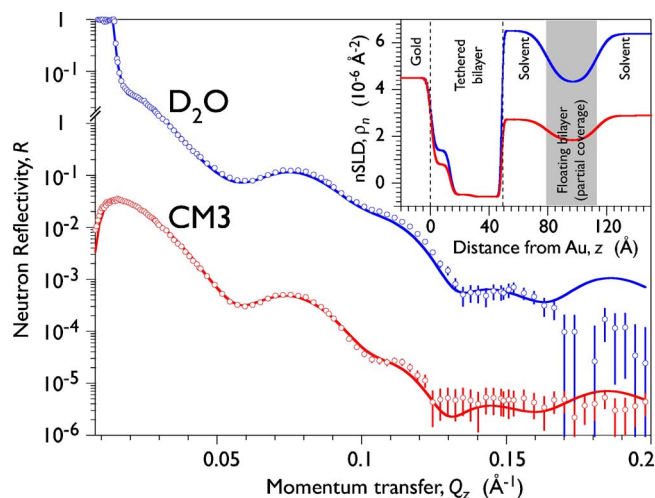
proximal layer, and led thus to an expansion of the hydrophobic slab (note that the extended tail lengths of any of the phospholipids was larger than that of WC14, with the exception of DMPC which was equal in hydrophobic tail length). It is then not surprising that all bilayer thickness values of stBLMs were larger than that of the 100% WC14 tBLM, with the exception of the stBLM completed with DMPC.

Uniquely for POPC, NR persistently revealed the formation of a secondary bilayer which was always incomplete (Fig. 9), with $\sim 10\% - 50\%$ coverage, depending on the individual sample. These overlayers remained stable when the solvent buffer was gently changed, e.g., for isotopic variation, and did not degrade over a period of 24 h. The secondary layer floated above the primary bilayer on a cushion of solvent with a thickness of ~ 35 Å, a gap similar to that observed in the "floating bilayers" characterized by Charitat *et al.*.[50] Difficulties arose where we tried to put the POPC results into the systematic progression of results with other

TABLE V. Best-fit parameters (model B) to electrochemical impedance spectra of stBLMs ($x_{WC14}=0.5$) completed with various phospholipids. Uncertainties, in parentheses, as obtained from the covariance matrices.

	Filler lipid			
Parameter	DPhyPC	DOPC	POPC	DMPC[a]
CPE$_{tBLM}$ [μF cm^{-2} s$^{(\alpha-1)}$]	0.827(5)	0.886(5)	0.966(6)	1.376(12)
α_{tBLM}	0.988(1)	0.986(1)	0.981(1)	0.977(1)
CPE$_{defect}$ [μF cm^{-2} s$^{(\alpha-1)}$]	1.92(6)	1.90(4)	3.50(4)	3.46(38)
α_{defect}	0.52(3)	0.50(4)	0.54(2)	0.48(1)
R_{defect} (kΩ cm^2)	146(13)	119(19)	75(4)	24.5(2.7)
Fit quality χ^2($\times 10^5$)	6.75	7.60	5.34	5.68

[a]For DMPC, the best fit was achieved by adding to the equivalent circuit, model B, an additional conductivity pathway that accounts for an intrinsic conductivity of the membrane. In this particular case, its value was R_m=427(41) kΩ cm^2.

lipids which did not form similar overlayers, since the model used to describe the POPC data was necessarily more complex and may yet still not have described the physical situation adequately. For example, it is not clear whether overlayers with 10%–50% coverage will be adequately described by a model that assumes lateral homogeneity within the in-plane coherence length of the spectrometer. The reported best-fit model parameters—notably $d_{bilayer} = 35-40$ Å for POPC stBLMs—need therefore be considered with caution. (More recently, we observed that such an overlayer can be quantitatively removed with a gentle flush with a 1:1 mixture of ethanol and water without removing phospholipid from the stBLM.)

IV. DISCUSSION

In the absence of βME, WC14-based tBLMs are electrically insulating but, with only ~5 vol % exchangeable solvent in the spacer region, do not show the constitution of the submembrane layer that is desirable for fully functional membrane protein incorporation. In addition, the thickness of the slab ($d_{sub} \sim 17$ Å) is smaller than the fully extended HEO length (~20 Å), consistent with the FT-IRRAS data which indicates disordered HEO segments. These results imply that disordered HEO fills the submembrane space to the almost complete exclusion of water. The alkyl tails in the SAM are tightly packed (from NR) and ordered (from FT-IRRAS), thus presenting a strongly hydrophobic surface to the bulk solution that promotes bilayer formation through either vesicle fusion or rapid solvent exchange. At the same time, however, it apparently hinders solvent exchange with the submembrane space.

Significant hydration of the submembrane space is achieved by backfilling with βME, leading to volume fractions of exchangeable water, x_{sub}^{water}, as high as 60–75 vol %, depending on the filler lipid. The significance of the neutron results is obvious, although it must be emphasized that standard deviations of x_{sub}^{water} in multiple independent measurements on samples of the same chemical constitution were in the range of 5%–10% (Table III). In the adsorption process, the βME competes with WC14 for Au occupancy sites, apparently reducing the packing density of WC14 on the surface. This hypothesis is supported by the near-linear reduction of the ellipsometric thickness of mixed βME:WC14 SAMs with increasing solution concentration of βME. It is clear, on the other hand, that WC14 maintains a significant presence at the surface even at low solution concentrations, as the surfaces appear only weakly hydrophilic (contact angle ~80° at 10% WC14). NR results suggest that the mixed monolayer collapses onto the surface in the presence of water at $x_{WC14} < 30\%$, presumably resulting in water exclusion from the alkyl tails. It is inferred from the steplike increase in capacitance (Fig. 6) of the mixed SAMs at 70% WC14 that the individual tethers are so far apart at this point that they no longer form a continuous surface layer.

In the adsorption process, WC14 appears to trap βME on the surface. Although the small molecule, βME, is essentially undetectable in the presence of WC14 with the charac-

terization methods at our disposal, and therefore cannot be reliably quantified, it is noted that the ellipsometric thickness of the mixed SAMs does not change with increasing incubation time of the deposition solution. If βME were thermodynamically favored on the surface, the ellipsometric thickness would decrease with increasing exposure time, while conversely, if the long-chain WC14 is thermodynamically favored, as expected,[51] then an increased incubation time would increase the ellipsometric thickness. Instead, the surface film forms rapidly to an ellipsometric thickness that depends on the ratio of the components in solution, and then remains constant. This suggests that WC14 is uniformly distributed across the surface, rather than forming isolated domains within a βME-covered surface. The near ideality of the CPE_{SAM} capacitance at all x_{WC14} ($\alpha_{SAM} > 0.98$) is also consistent with lateral homogeneity of the surface films.

The reduction in WC14 density in the surface film upon backfilling appears to be partially compensated for by an increase in the surface area that each WC14 molecule occupies in an stBLM, as the thickness of the submembrane space decreases with x_{WC14}, to only $d_{sub} \sim 12$ Å for an stBLM with $x_{WC14} = 30\%$. Nevertheless the structural similarities of DPhyPC stBLMs formed on SAMs with varying x_{WC14} indicate that the inner leaflet of the bilayer is "filled in" by the lipid. This suggests that the stBLM is more representative of a membrane model composed purely of natural lipids than tBLMs with a completely synthetic inner leaflet. On the other hand, measurements of the electrochemical behavior of the mixed monolayers before exposure to lipid and after ethanol rinsing, which removes the bilayer, are essentially identical. We surmise that the tethering molecules themselves are not perturbed by the addition of lipid. In addition, this procedure allows the stBLMs to be reused in multiple preparations after a simple ethanol wash.

An important advantage of the system presented here is that the bilayer membrane can be reliably formed, quite simply and with comparable results, for a range of different lipids. Although not yet exhaustively tested, we have so far not encountered any restriction on the extension of the sample preparation procedure to lipid mixtures. In fact, we have prepared mixed stBLMs with dipolar and charged lipids or stBLMs entirely from charged lipid (data not shown). The protocol is obviously applicable to yield membranes with more complex constitutions. This also includes the incorporation of components such as sterols. The only filler lipid that yielded stBLMs with somewhat compromised electrical properties (but intact structures, as seen in NR) was DMPC. DMPC-based stBLMs also had the highest density of membrane defects. This deficiency may be partially due to preparing and characterizing samples at (21 ± 1) °C, near the transition temperature, $T_c \sim 24$ °C, of free DMPC bilayers from the liquidlike L_α to the liquid-crystalline P_β ripple phase.[52] Structural frustration may then result from the incompatibility of the tether-enforced planarity of the stBLM and the P_β structure whose ripple amplitude is well above the short length of the HEO spacer. Alternatively, the pre-

sumed proximity of the phase transition—the actual T_c in the stBLMs is unknown—might simply result in domain boundaries between the coexisting phases.

A final point concerns the fluidity of the bilayer membrane as a function of the density of surface tethers. An important feature of biological membranes, captured as early as in the 1972 *fluid mosaic model*[53] and elaborated in the Saffman-Delbrück model of anisotropic diffusion,[54] is that the two-dimensional molecular motion within the membrane matrix is rapid and unhindered. Chemical tethering of the inner tBLM leaflet obviously restricts diffusion of the lipids directly tethered and may impede the diffusion of other species incorporated in the bilayer. Reducing the proportion of tethered molecules is expected to increase this mobility, again leading to a more biologically relevant system. Although neither NR nor EIS is sensitive to molecular mobility, we do have indirect evidence for dynamic flexibility in st-BLMs. Firstly, by monitoring structural defects through their amplification by phospholipase enzyme activity, we demonstrated that stBLMs show largely different turnover rates depending on their composition of unsaturated (POPC) or branched (DPhyPC) lipids.[55] Secondly, in the work reported here, the exchange of solvent in the submembrane space with the bulk is also likely dependent on dynamic defects. While the density of Ohmic defects remains within an order of magnitude upon going from a fully tethered membrane to an stBLM (70 mm^{-2} vs 350 mm^{-2} according to EIS), the solvent transfer compliance of the two systems is entirely different, with the fully tethered bilayer *much more* than an order of magnitude in time higher in its resistance against solvent exchange. We attribute the observed efficient replacement of solvent isotopes across the membrane to the formation of transient defects that should correlate with lipid mobility.

V. CONCLUSIONS AND OUTLOOK

We have developed and characterized a simple, but highly flexible and robust biomimetic membrane system, the sparsely tethered bilayer lipid membrane, for studies and applications of biological membranes. stBLMs are long-term stable, electrically sealing, and laterally homogeneous on the molecular length scale. The protocol can be easily extended to the preparation of mixed membranes and to surfaces with controlled charge density. The approach can be scaled to large and small surface areas. The two-step formation of the bilayer membrane (producing first a stable SAM, followed by noncovalent membrane completion with any from a range of saturated and unsaturated lipids, or lipid mixtures) and reversibility of membrane formation imply that SAMs may be recycled and reused. The robustness and flexibility of the system make it amenable to various characterization techniques and potentially useful in many biomimetic metrologies, including biosensors.

System characterization using primarily EIS and NR demonstrated the synergy of the two techniques. EIS provided the capability to rapidly screen different sample conditions and compositions for function. NR enabled us to verify the stBLM structure and provided direct evidence for the presumed molecular stratification of the system. Moreover, with isotopic contrast variation, NR permitted a quantitative assessment of the chemical composition of the molecular architecture. This allowed the determination of the molecular-scale dimension and level of hydration of the submembrane space, which has so far mostly been indirectly inferred upon in previous work. The molecular constitution of this space is considered crucial for the use of membrane mimics as platforms for studies of transmembrane proteins[14] and their applications. Our work shows, quantitatively for the first time, how submembrane space hydration depends on backfilling the tether lipids to reduce their density on the surface.

Optical microscopy-based characterization of similar systems has established determinants of their lateral homogeneity on the length scale of visible light[12,16,17] and has quantified their in-plane fluidity.[11,12,17,56] In the systems we described here, we have thus far only qualitatively assessed the in-plane fluidity in simple photorecovery experiments and have observed diffusion coefficients that are of the order of a few 10^{-8} cm^2/s. While these properties have not yet been rigorously quantified in a well-controlled optical configuration in our laboratory, work is underway toward that end. Moreover, we have been successful in incorporating a large protein, viz. the α-toxin of *Staphylococcus aureus*, a heptameric transmembrane pore with a molecular weight of ~230 kDa, in high lateral densities in the fully functional state.[27] In fact, the protein has been incorporated in such quantities that we are now able to determine structural properties within this intrinsically disordered multicomponent membrane system in unprecedented detail. This yields previously inaccessible experimental results on protein-membrane interactions[27] that have so far at best been inferred from molecular simulations.

tBLMs formed on sparsely tethered SAMs are promising model membranes of biological relevance. A relatively small proportion of tethered molecules allows the inner and outer leaflets to become more symmetric, leading to lateral transport properties within the stBLM that are presumably closer to those of free bilayer membranes than would be possible in a fully tethered membrane. The ease and adaptability of the stBLM system allow it to be custom tailored to studies of a variety of membrane-associated proteins, which will constitute the ultimate test for its relevance to biological studies.

NOMENCLATURE

BLM	bilayer lipid membrane
tBLM/stBLM	tethered bilayer lipid membrane/sparsely tethered bilayer lipid membrane
SAM	self-assembled monolayer
WC14	20-tetradecyloxy-3,6,9,12,15,18,22-heptaoxahexatricontane-1-thiol
EO	ethylene oxide
HEO/OEO/PEG	hexa(ethylene oxide)/oligo(ethylene oxide)/poly(ethylene oxide)
βME	β-mercaptoethanol

DPhyPC   1,2-diphytanoyl-
                        sn-glycero-3-phosphatidylcholine
DOPC   1,2-dioleoyl-
                        sn-glycero-3-phosphatidylcholine
POPC   1-palmitoyl-2-oleoyl-
                        sn-glycero-3-phosphatidylcholine
DMPC   1,2-dimyristoyl-
                        sn-glycero-3-phosphatidylcholine
Tris-HCl   (tris(hydroxymethyl) aminomethane-HCl
EI/EIS   electrochemical impedance/
                        electrochemical impedance spectroscopy
NR   neutron reflection
FT-IRRAS   Fourier-transform infrared reflection ab-
                        sorption spectroscopy
SPR   surface plasmon resonance
AFM   atomic force microscopy
AND/R   Advanced Neutron
                        Diffractometer/Reflectometer
nSLD   neutron scattering length density
CPE   constant phase element

ACKNOWLEDGMENTS

[1] M. Tanaka and E. Sackmann, Nature (London) **437**, 656 (2005).
[2] C. Erdelen *et al.*, Langmuir **10**, 1246 (1994).
[3] E. Sackmann, Science **271**, 43 (1996).
[4] C. A. Naumann, O. Prucker, T. Lehmann, J. Rühe, W. Knoll, and C. W. Frank, Biomacromolecules **3**, 27 (2002).
[5] B. A. Cornell, V. L. B. Braach-Maksvytis, L. B. King, P. D. J. Osman, B. Raguse, L. Wieczorek, and R. J. Pace, Nature (London) **387**, 580 (1997).
[6] C. W. Meuse, S. Krueger, C. F. Majkrzak, J. A. Dura, J. Fu, J. T. Connor, and A. L. Plant, Biophys. J. **74**, 1388 (1998).
[7] Y. L. Cheng, N. Boden, R. J. Bushby, S. Clarkson, S. D. Evans, P. F. Knowles, A. Marsh, and R. E. Miles, Langmuir **14**, 839 (1998).
[8] M. L. Wagner and L. K. Tamm, Biophys. J. **79**, 1400 (2000).
[9] R. Naumann *et al.*, Langmuir **19**, 5435 (2003).
[10] S. Terrettaz, M. Mayer, and H. Vogel, Langmuir **19**, 5567 (2003).
[11] C. Rossi, J. Homand, C. Bauche, H. Hamdi, D. Ladant, and J. Chopineau, Biochemistry **42**, 15273 (2003).
[12] F. Albertorio, A. J. Diaz, T. Yang, V. A. Chapa, S. Kataoka, E. T. Castellana, and P. S. Cremer, Langmuir **21**, 7476 (2005).
[13] L. J. C. Jeuken, S. D. Connell, P. J. F. Henderson, R. B. Gennis, S. D. Evans, and R. J. Bushby, J. Am. Chem. Soc. **128**, 1711 (2006).
[14] M. Tanaka, MRS Bull. **31**, 513 (2006).
[15] L. Zhang and S. Granick, MRS Bull. **31**, 527 (2006).
[16] C. Hamai, T. Yang, S. Kataoka, P. S. Cremer, and S. M. Musser, Biophys. J. **90**, 1241 (2006).
[17] V. Kiessling, J. M. Crane, and L. K. Tamm, Biophys. J. **91**, 3313 (2006).
[18] Y. Fang, Y. Hong, B. Webb, and J. Lahiri, MRS Bull. **31**, 541 (2006).
[19] S. Daniel, F. Albertorio, and P. S. Cremer, MRS Bull. **31**, 536 (2006).
[20] I. Burgess, M. Li, S. L. Horswell, G. Szymanski, J. Lipkowski, J. Majewski, and S. Satija, Biophys. J. **86**, 1763 (2004).
[21] B. W. Koenig, S. Krueger, W. J. Orts, C. F. Majkrzak, N. F. Berk, J. V. Silverton, and K. Gawrisch, Langmuir **12**, 1343 (1996).
[22] G. Krishna, J. Schulte, B. A. Cornell, R. Pace, L. Wieczorek, and P. D. Osman, Langmuir **17**, 4858 (2001).
[23] G. Krishna, J. Schulte, B. A. Cornell, R. J. Pace, and P. D. Osman, Langmuir **19**, 2294 (2003).
[24] B. Raguse, V. L. B. Braach-Maksvytis, B. A. Cornell, L. B. King, P. D. J. Osman, R. J. Pace, and L. Wieczorek, Langmuir **14**, 648 (1998).
[25] D. J. Vanderah, R. S. Gates, V. Silin, D. N. Zeiger, J. T. Woodward, C. W. Meuse, G. Valincius, and B. Nickel, Langmuir **19**, 2612 (2003).
[26] S. M. Schiller, R. Naumann, K. Lovejoy, H. Kunz, and W. Knoll, Angew. Chem., Int. Ed. **42**, 208 (2003).
[27] D. J. McGillivray, G. Valincius, F. Heinrich, J. W. F. Robertson, D. J. Vanderah, W. Febo-Ayala, I. Ignatjev, M. Lösche, and J. J. Kasianowicz (submitted).
[28] Certain commercial materials, equipment, and instruments are identified in this paper in order to specify the experimental procedure as completely as possible. In no case does such identification imply a recommendation or endorsement by the National Institute of Standards and Technology, nor does it imply that the materials, equipment, or instruments identified are necessarily the best available for the purpose.
[29] See EPAPS Document No. E-BJIOBN-2-001701 for a complete description of the synthesis and characterization of 20-tetradecyloxy-3 6, 9, 12, 15, 18, 22-heptaoxahexatricontane-1-thiol (WC14). This document can be reached via a direct link in the online article's HTML reference section or via the EPAPS homepage (http://www.aip.org/pubservs/epaps.html).
[30] D. J. Vanderah, C. W. Meuse, V. Silin, and A. L. Plant, Langmuir **14**, 6916 (1998).
[31] I. D. Raistrick, D. R. Franceschetti, and J. R. Macdonald, in *Impedance Spectroscopy: Theory, Experiment, and Applications*, edited by E. Barsoukov and J. R. Macdonald (Wiley, New York, 2005), p. 27.
[32] R. K. Burstein, Elektrokhimiya **3**, 349 (1967).
[33] J. Penfold, Curr. Opin. Colloid Interface Sci. **7**, 139 (2002).
[34] J. A. Dura *et al.*, Rev. Sci. Instrum. **77**, 074301 (2006).
[35] P. A. Kienzle, M. Doucet, D. J. McGillivray, K. V. O'Donovan, N. F. Berk, and C. F. Majkrzak (2000–2006), http://www.ncnr.nist.gov/reflpak
[36] L. G. Parratt, Phys. Rev. **95**, 359 (1954).
[37] www.ncnr.nist.gov/resources/n-lengths/list.html
[38] D. A. Doshi, E. B. Watkins, J. N. Israelachvili, and J. Majewski, Proc. Natl. Acad. Sci. U.S.A. **102**, 9458 (2005).
[39] D. A. Lowy and H. O. Finklea, Electrochim. Acta **42**, 1325 (1997).
[40] C. Steinem, A. Janshoff, W. P. Ulrich, M. Sieber, and H. J. Galla, Biochim. Biophys. Acta **1279**, 169 (1996).
[41] The contribution of the Helmholtz layer is estimated as $C'_{SAM}=(C_{SAM}^{-1}+C_H^{-1})^{-1}$, where C'_{SAM} is the corrected SAM capacitance and $C_H \approx 10\ \mu\text{F cm}^{-2}$. We estimate the relative uncertainty, due to uncertainty in C_H, $\Delta C'_{SAM} \approx 10\%$.
[42] M. D. Porter, T. B. Bright, D. L. Allara, and C. E. D. Chidsey, J. Am. Chem. Soc. **109**, 3559 (1987).
[43] P. Harder, M. Grunze, R. Dahint, G. M. Whitesides, and P. E. Laibinis, J. Phys. Chem. B **102**, 426 (1998).
[44] M. A. K. Dissanayake and R. Frech, Macromolecules **28**, 5312 (1995).
[45] D. J. Vanderah, J. Arsenault, H. La, R. S. Gates, V. Silin, C. W. Meuse, and G. Valincius, Langmuir **19**, 3752 (2003).
[46] V. M. Kaganer, H. Möhwald, and P. Dutta, Rev. Mod. Phys. **71**, 779 (1999).
[47] A more complete rationalization of this model will be given elsewhere [G. Valincius and F. Ivanauskas (unpublished)].
[48] R. De Levie, Electrochim. Acta **8**, 751 (1963).
[49] H. Keiser, K. D. Beccu, and M. A. Gutjahr, Electrochim. Acta **21**, 539 (1976).
[50] T. Charitat, E. Bellet-Amalric, G. Fragneto, and F. Graner, Eur. Phys. J. B **8**, 583 (1999).
[51] C. D. Bain and G. M. Whitesides, J. Am. Chem. Soc. **110**, 3665 (1988).
[52] D. Needham and E. Evans, Biochemistry **27**, 8261 (1988).
[53] S. J. Singer and G. L. Nicolson, Science **173**, 720 (1972).
[54] P. G. Saffman and M. Delbrück, Proc. Natl. Acad. Sci. U.S.A. **72**, 3111 (1975).
[55] G. Valincius, D. J. McGillivray, W. Febo-Ayala, D. J. Vanderah, J. J. Kasianowicz, and M. Lösche, J. Phys. Chem. B **110**, 10213 (2006).
[56] L. Zhang and S. Granick, Proc. Natl. Acad. Sci. U.S.A. **102**, 9118 (2005).